Absorption of spherical bubbles in a square microchannel

David MIKAELIAN*, Benoît HAUT, Louise DE CANNIERE, Benoit SCHEID

* Corresponding author: Email: dmikaeli@ulb.ac.be
Laboratory Transfers, Interfaces and Processes (TIPs), CP 165/67,
Université Libre de Bruxelles, Av. F. D. Roosevelt 50, 1050 Brussels, Belgium

Abstract Microfluidics is a fast growing field in which the manipulation of bubbles in liquid phase is of utmost importance. In this paper, the absorption of spherical bubbles in a square microchannel is investigated for a bubbly flow. Numerical simulations of the gas-liquid two-phase flow and the mass transfer around spherical bubbles in a square microchannel are carried out. Correlations are established for the bubble velocity and the mass transfer rate. A model for the dissolution of spherical bubbles along a square microchannel is proposed in the case of the bubbly flow regime and validated using existing experimental data. This model can be used, for instance, for designing microabsorbers for lab-on-a-chip applications.

Keywords: Microfluidics, Absorption, Square microchannel, Bubbly flow, Spherical bubbles.

1. Introduction

Nowadays, microfluidic devices are increasingly used. Indeed, they enable using less reactant, having a deep control on the involved processes, lowering the risk due to the use of high quantity of hazardous materials and being easily handled. Microfluidic devices involving gas-liquid two-phase flows in microchannels are encountered in many circumstances such as gas-liquid absorption. Gas-liquid two-phase flow patterns were investigated in Cubaud and Ho (2004) and in Kim et al. (2011) for square and rectangular microchannels. In both papers, five main gas-liquid two-phase flow regimes were reported as a function of the gas and liquid superficial velocities and named, after Cubaud and Ho (2004), as: bubbly, wedging, slug, annular and dry flows. The bubbly flow corresponds to discrete spherical bubbles with diameters smaller than the channel height and moving in a continuous liquid phase. The mass transfer around gas bubbles for different two-phase flow regimes was studied in square and rectangular microchannels (Kashid et al. (2011), Sun and Cubaud (2011), Cubaud et al. (2012)). These studies mainly focused on the slug flow, and the transition to bubbly flow was only observed in the experiments by Cubaud et al. (2012).

To the best of our knowledge, the gas-liquid two-phase flow and the mass transfer around bubbles in square microchannels for the bubbly flow regime have not been analyzed yet, neither theoretically neither numerically. The aim of the present work is therefore to fill the gap by developing a numerical procedure in order to simulate the gas-liquid two-phase flow and the mass transfer around spherical bubbles in a square microchannel. Correlations for the bubble velocity and the mass transfer rate around spherical bubbles in a square microchannel are proposed and a model describing the dissolution of spherical bubbles along a square microchannel is presented, and compared to available experimental data.

2. Problem statement

A square microchannel of length L_c and width w is considered. A segment of this microchannel with a length L and containing, at its center, a spherical bubble of diameter d is studied. Taking benefit of symmetries, only a quarter of the microchannel is analyzed. It is described in Fig. 1, including the labels of the boundaries and notations.

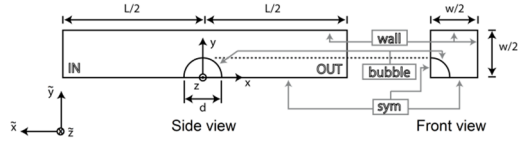

Figure 1: Computational domain for modelling a spherical bubble in a segment of a square microchannel.

In the laboratory reference frame $(\tilde{x},\tilde{y},\tilde{z})$, the bubble moves through the microchannel with a velocity V_B in the positive $\tilde{x}$ direction. The liquid and gas mixture moves with a total superficial velocity J_A in the same direction. J_A is equal to $(Q_L + Q_G)/w^2$, with Q_L and Q_G the volumetric liquid and gas flow rates, respectively. The reference frame attached to the center of the bubble (x,y,z) moves at the bubble velocity V_B in the positive $\tilde{x}$ direction. Therefore, in (x,y,z), the bubble is stationary, the liquid-gas mixture moves with a velocity $V_B - J_A$ in the positive x direction and the walls of the microchannel move with a velocity V_B in the positive x direction.

As the density and the viscosity of the liquid are much higher than those of the gas, a one-sided approach is used where only the liquid flow is considered and the bubble is a spherical hole in the computational domain with a mass flux at its surface. The liquid flow and the mass transfer around the bubble inside the square microchannel are analyzed by solving, in (x,y,z), the continuity, the Navier-Stokes and the mass transport equations in stationary conditions.

The boundary conditions for the liquid flow and the mass transport are presented in Table 1. Periodic boundary conditions are used between the IN and the OUT planes in order to reproduce the chain of bubbles that are generated in real microchannels. Therefore, a pressure difference ΔP and a concentration difference ΔC exist between the IN and the OUT planes and are parts of the computational unknowns. As periodic conditions are used, L represents the distance between two successive bubbles.

Boundary	**Boundary conditions for the liquid flow**	**Boundary conditions for the mass transport**
wall	Moving with a velocity $(V_B, 0, 0)$ with a no slip condition	No mass flux
bubble	Undeformable and stationary surface with a stress-free condition	Saturation concentration C_{sat}
sym	Symmetry conditions	Symmetry conditions
IN and OUT	Periodic conditions with a mass flow rate equal to $(V_B - J_A)\rho w^2$	Periodic conditions with an average concentration equal to C_{bulk} on the plane IN

Table 1: Boundary conditions for the liquid flow and the mass transport.

Three non-dimensional control parameters are used: d/w, $Re_{J_A} = \frac{\rho J_A w}{\mu}$ and $Sc = \frac{\mu}{\rho D}$, with ρ the density of the liquid [kg/m^3], μ the dynamic viscosity of the liquid [Pa s] and D the diffusion coefficient of the dissolved gas [m^2/s]. The ranges covered by these three non-dimensional control parameters are $0.15 \leq d/w \leq 0.75$, $5.74 \leq Re_{J_A} \leq 28.7$ and $150 \leq Sc \leq 550$. These ranges ensure covering the realistic values of the parameters encountered for usual gas and liquid combinations. Two non-dimensional variables are defined for the post-processing: V_B/J_A and the Sherwood number $Sh = \frac{k_l d}{D}$, with k_l the mass transfer coefficient across the bubble interface.

3. Numerical procedure

Based on the computational domain of Fig. 1, a grid is generated for each value of d/w using the software Gambit 2.4. Refined zones for the mesh are used around the bubble and next to the walls to ensure that the diffusion boundary layers are correctly captured. The grid independence is checked for each value of d/w.

For each generated grid, the system of equations defining the problem is solved in stationary conditions in the liquid phase with the boundary conditions of Table 1. The three-dimensional version with a double precision of the solver Ansys Fluent 14.5 is used for this purpose.

The steady bubble velocity V_B implies that the x-component of the force F_x exerted by the liquid on the bubble surface should be equal to zero. It provides a relation between J_A and V_B. Here, J_A is imposed (through Re_{J_A}) and V_B is then evaluated such that F_x vanishes. From the numerical results of the mass transport, the mass transfer coefficient k_l is calculated by dividing the mass flow rate at the bubble surface by the bubble surface area and by the driving concentration difference $C_{sat} - C_{bulk}$. The length of the computational domain L is adjusted to a value, depending on d, J_A and D, such that when L is increased by 200 µm, the relative

change in k_l is lower than 1%.

4. Correlations

Based on the form of the correlation of Cubaud et al. (2012) and the limiting values of V_B/J_A for $d \to 0$ and $d \to \infty$, a form of correlation is proposed for V_B/J_A and fitted to the numerical results. It leads to

$$\frac{V_B}{J_A} = 1 + 1.1\exp\left[-\left(\frac{d}{w}\right)^5\right] . \quad (1)$$

Based on the form of well-known relation of Levich (1962) to express Sh for the creeping flow around spheres with a stress-free condition, a form of correlation is proposed for Sh and fitted to the numerical results. It leads to

$$Sh = 2 + 3Re^{1/3}Sc^{1/3}\frac{d}{w} , \quad (2)$$

with $Re = Re_{J_A}\frac{V_B}{J_A}\frac{d}{w}$.

Equations (1) and (2) are established and valid for the range of control parameters given in section 2.

5. Model for the bubble dissolution

The liquid fraction α_L is defined as

$$\alpha_L = \frac{Q_L}{Q_L+Q_G}. \quad (3)$$

In order to calculate α_L at a coordinate x along the microchannel, the bubble at the coordinate x and the preceding one are considered with $l(x)$ the distance between the centers of these two bubbles, as represented in Fig. 2. By definition, $Q_L + Q_G = J_A w^2$ and $Q_G = \frac{\pi d(x)^3}{6\,l(x)}V_B(x)$, the introduction of which in Equation (3) leads to:

$$\alpha_L(x) = 1 - \frac{\pi d^3(x)}{6w^2 l(x)}\frac{V_B(x)}{J_A(x)} , \quad (4)$$

in which $V_B(x)/J_A(x)$ is calculated using Equation (1).

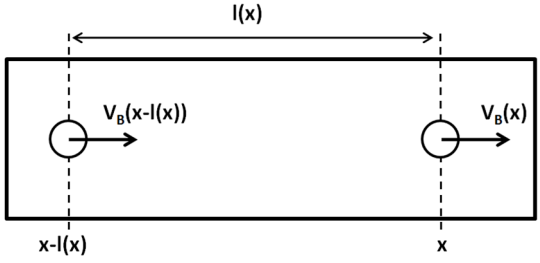

Figure 2: Representation of two successive bubbles in the microchannel.

The variation of Q_L along the microchannel can be neglected as the density of the gas is much lower than the density of the liquid.

It is assumed here that the relative variation of $l(x)$ is equal to the relative variation of V_B, which leads to

$$l'(x) = \frac{V_B'(x)l(x)}{V_B(x)} . \quad (5)$$

The pressure drop in the liquid phase ΔP along a square microchannel for a laminar one-phase flow at a superficial velocity $J_L = Q_L/w^2$ can be calculated by

$$\Delta P \equiv \frac{1}{2}\frac{f}{w}\rho J_L^2 L_c = \frac{\gamma\mu J_L L_c}{2w^2} , \quad (6)$$

where $f = {}^{\gamma\mu}/_{\rho J_L w}$ is the friction factor and γ is a constant equal to 56.8 for a square channel (Bruus (2008)). The pressure drop $\Delta P_{2-phase}$ for a two-phase bubbly flow (characterized by α_L close to unity) along the (same) square microchannel can be evaluated by

$$\Delta P_{2-phase} \equiv \frac{\Delta P}{\alpha_L} = \frac{\gamma\mu J_L L_c}{2w^2\alpha_L} , \quad (7)$$

which has been shown by Cubaud and Ho (2004) to be valid. Assuming a linear pressure drop along the microchannel, the pressure in the liquid phase along the microchannel can be computed using

$$p'(x) = -\frac{\gamma\mu J_L}{2w^2\alpha_L(x)} . \quad (8)$$

The pressure in the gas phase p_G can be calculated from the pressure in the liquid phase using the Young-Laplace equation:

$$p_G = p(x) + \frac{4\sigma}{d(x)}, \quad (9)$$

where σ is the surface tension of the gas-liquid interface.

A mass balance for the transferred species between the gas phase and the liquid phase written for a control segment of length Δx leads, for $\Delta x \to 0$, to the following equation describing the evolution of the concentration of the dissolved gas in the liquid phase (C) along the microchannel:

$$C'(x) = \frac{-\alpha_L(x)p_G'(x)+\alpha_L'(x)p_G(x)+\alpha_L^2(x)p_G'(x)}{\alpha_L^2(x)RT} , \quad (10)$$

with T the temperature (supposed constant in this work) and R the gas constant.

The change of the diameter of a bubble along a microchannel is due to the mass transfer between the bubble and the liquid

phase and the bubble expansion due to the pressure decrease along the microchannel, and is described by:

$$\frac{p'_G(x)d(x)+3p_G(x)d'(x)}{6RT} = -\frac{1}{V_B(x)}k_l(x)(Hp_G(x) - C(x)), \quad (11)$$

where H is the Henry coefficient of the dissolved gas and $k_l(x)$ is evaluated using Equation (2) and the definition of Sh.

To summarize, the complete model for the dissolution of spherical bubbles along a square microchannel in the bubbly flow regime consists of:

- four first-order ordinary differential equations (Equations (5), (8), (10) and (11));
- the Young-Laplace equation (Equation (9));
- the relation for α_L (Equation (4));
- the correlations for V_B/J_A (Equation (1)) and for Sh (Equation (2)).

Four boundary conditions are necessary for the first-order ordinary differential equations. These conditions are the values of l, p, C and d at the position $x = 0$, which are denoted l_0, p_0, C_0 and d_0, respectively.

6. Comparison to the literature

The experimental data of Cubaud et al. (2012) can be used in order to validate the model for the dissolution of spherical bubbles along a square microchannel. Indeed, in the work of Cubaud et al. (2012), a bubbly flow is observed in a nearly square microchannel during a part of their experiments for the dissolution of CO_2 in water at room temperature and atmospheric pressure. The microchannel has a width $w_c = 87$ µm, a height $h_c = 100$ µm and a length $L_c \approx 10$ cm. In the experimental data of Cubaud et al. (2012), t, α_L, V_B/J_A and d are recorded along the microchannel every 0.755 ms. These data are adapted in order to be able to compare them to the results computed with our model. The time t is converted to the coordinate x using a constant V_B for a time interval. In the work of Cubaud et al. (2012), α_L is evaluated by $1 - \frac{\pi d^3}{6 w_C h_C l}$ instead of $1 - \frac{\pi d^3}{6 w_C h_C l}\frac{V_B}{J_A}$. It has been corrected here. The ratio V_B/J_A of Cubaud et al. (2012) has also been corrected because J_A is evaluated by $J_A = J_L/\alpha_L$. As the microchannel is nearly square, w in the model is taken equal to its hydraulic diameter: $w = \frac{2 w_c h_c}{w_c + h_c}$. Only the parts of the experiments of Cubaud et al. (2012) where $d/w \leq 0.75$ is considered (see Fig. 3). The coordinate $x = x_0$ along the microchannel where $d/w = 0.75$ is used in the model as the inlet of the microchannel. The length of the microchannel L_{out} used in the model is calculated by $L_{out} = L_C - x_0$.

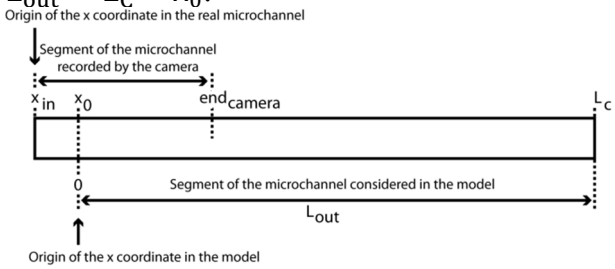

Figure 3: Sketch of the real microchannel, the segment considered in the model and the segment recorded by the camera in Cubaud et al. (2012).

From the adapted data of Cubaud et al. (2012), the boundary conditions l_0, p_0, C_0 and d_0 are determined: d_0 is equal to $0.75w$, l_0 is calculated from the non corrected version of α_L at the coordinate x_0 by $l_0 = \frac{\pi d_0^3}{6 w_C h_C (1-\alpha_L(x_0))}$, p_0 is adjusted such that $p(L_{out}) = 101325$ Pa and C_0 is calculated by $C_0 = \frac{1-\alpha_L(x_{in})}{\alpha_L(x_{in})}\frac{p(x_{in})}{RT} - \frac{1-\alpha_L(x_0)}{\alpha_L(x_0)}\frac{(p_0 + 4\sigma/d_0)}{RT}$, with "$x_{in}$" the inlet position of the real microchannel.

The system of equations of the complete dissolution model described in Section 5 is solved with the boundary conditions given above for a square microchannel having the same hydraulic diameter as the microchannel of Cubaud et al. (2012) and a length L_{out}. The computed values of d/w, α_L and V_B/J_A along the microchannel are compared to the experimental values of Cubaud et al. (2012) in Fig. 4.

The agreement is good between the computed and the experimental results for d/w and α_L. The small deviation between them can be explained by the fact that the bubble separation distances are smaller in the

experiments than in the numerical simulations and thus the mass transfer around the bubbles is influenced by the preceding bubbles. An accurate value for L_c is not provided in the work of Cubaud et al. (2012) and thus the value of 10 cm used in the model is maybe not accurate enough. For V_B/J_A, a difference up to 15% is observed between the numerical results and the experimental ones. This deviation could be explained by the fact that the bubble interface is maybe not perfectly clean in the experiments, which would invalidate the stress-free boundary condition used in the model. Another source of discrepancy can arise here from the fact that the correlations established for V_B/J_A and Sh are obtained for a square microchannel and not for a rectangular one as in the experiments of Cubaud et al. (2012).

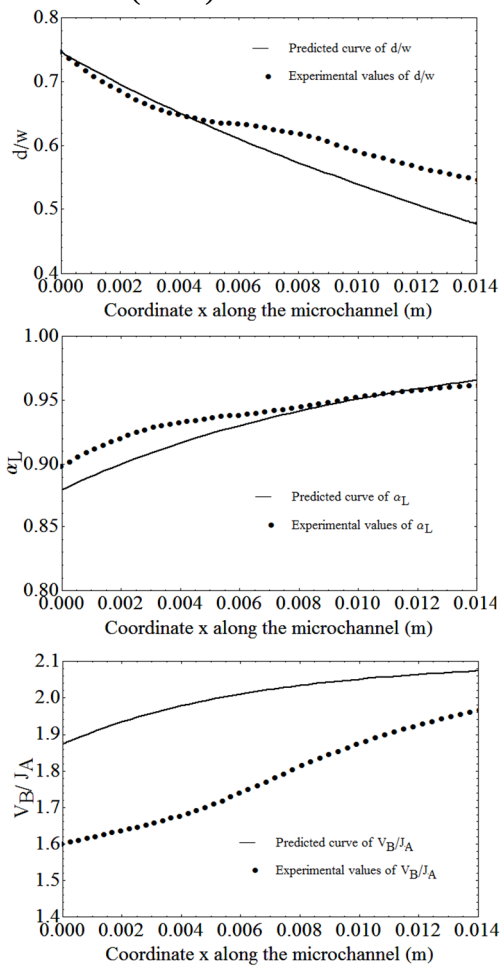

Figure 4: Comparison between the values of d/w, α_L and V_B/J_A computed with the model and the experimental results of Cubaud et al. (2012) for $Q_L = 110\,\mu l/min$. x_0 is subtracted to the x coordinate of the experimental results and only the part of the microchannel where the images are recorded is considered for the comparison.

7. Conclusion

The gas-liquid two-phase flow and the mass transfer around spherical bubbles in a square microchannel are studied numerically in this work. Correlations are established for V_B/J_A and Sh. A model for the dissolution of spherical bubbles along a square microchannel in the bubbly flow regime is proposed. A quite good agreement is observed between the numerical results predicted using this model and the experimental data of Cubaud et al. (2012). It can be seen as a validation for the dissolution model as well as for the correlations for V_B/J_A and Sh (Equations (1) and (2)).

The proposed correlations and model for the dissolution of spherical bubbles can be applied for square microchannels of various sizes and for various combinations of gas and liquid. They are used, for instance, for designing a lab-on-a-chip device for the absorption of O_2 or H_2 in methanol (to be published).

Acknowledgements

The authors acknowledge the Fonds de la Recherche Scientifique (F.R.S.-F.N.R.S.) for its financial contribution. This research has been performed under the umbrella of the COST action MP1106 and also takes part in the Inter-university Attraction Pole Programme (IAP 7/38 MicroMAST) initiated by the Belgian Science Policy Office.

References

T. Cubaud and C.M. Ho. Transport of bubbles in square microchannels. Physics of Fluids, 16, 4575 (2004).

N. Kim, E.T. Evans, D. S. Park, S. A. Soper, M. C. Murphy, D. E. Nikitopoulos. Gas-liquid two-phase flows in rectangular polymer micro-channels. Experiments in Fluids, 51(2), 373-393 (2011).

M. N. Kashid, A. Renken and L. Kiwi-Minsker. Gas-liquid and liquid-liquid mass transfer in microstructured reactors. Chemical Engineering Science, 66(17), 3876-3897

(2011).
R. Sun, and T. Cubaud. Dissolution of carbon dioxide bubbles and microfluidic multiphase flows. Lab on a Chip, 11(17), 2924-2928 (2011).
T. Cubaud, M. Sauzade and R. Sun. CO_2 dissolution in water using long serpentine microchannels. Biomicrofluidics, 6, 022002 (2012).
H. Bruus. Theoretical microfluidics (Vol. 18). Oxford University Press, 75 (2008).
V.G. Levich. Physicochemical hydrodynamics (Vol. 689). Englewood Cliffs, NJ: Prentice-Hall, 84-85 and 467 (1962).
R. B. Bird, W. E. Stewart, E. N. Lightfoot. Transport phenomena. John Wiley and Sons, 636 and 677-678 (2007).